Preprints of the 19th World Congress
The International Federation of Automatic Control
Cape Town, South Africa. August 24-29, 2014

Modeling Method for Electro-Rheological Dampers ⋆

Carlos A. Vivas-López * Diana Hernández-Alcantara * Ruben Morales-Menendez * Adriana Martínez Vargas *

* *Tecnológico de Monterrey, Av. Garza Sada # 2501, 64849, Monterrey México {a00794204, a00469139, rmm, adriana.mtz.vargas }@itesm.mx*

Abstract: A method for modeling *Electro-Rheological* (*ER*) dampers is proposed. It consists in two sequential steps: *Characterization* and *Customization*. Both steps are based on the observed dynamic behavior of the *ER* damper. The method requires experimental data of the damper, which is subjected to an specific *Design of Experiment* (*DoE*). The resulting equation includes the minimum terms to represent the real behavior of the damper, it can be implemented in an embedded system. The method was validated experimentally with a commercial *ER* damper; also, the customized model was quantitatively and qualitatively compared with a well-known *Eyring*-plastic model resulting with a 28% better performance based on the *Error to Signal Ratio* (*ESR*) performance index.

Keywords: Vehicle Dynamics, Chassis Control, Vehicles, Active Vehicle Suspension, Active Control

1. INTRODUCTION

Semi-Active (*SA*) suspension systems are capable to modify the amount of energy that can dissipate. This change can be done by means of an *Electro-Rheological* (*ER*) damper. This type of dampers are filled with a mixture of low viscosity oil and electric-field sensitive particles. The *ER* fluid behaves as a *Bingham* plastic material in presence of an electric field. This means, that ideally it behaves as a solid at low stress forces, but flows as a viscous fluid when this force reaches its yield stress. The yield stress is field dependent, it increases as the electric field does. This effect is caused by the molecules that align to the electric field, increasing the fluid flow resistant.

To predict the non-linear behavior of the *ER* damper, an accurate mathematical model is required. Most of the existing contributions consider parametric models, e.g. (Stanway et al., 1996; Dixon, 2007; Hong et al., 2005; Choi et al., 2008; Nguyen and Choi, 2009); however, there are also contributions with non-physical meaning (non-parametric) e.g. (Chen and Wei, 2006; Bitman et al., 2005; Nguyen and Choi, 2012). Some of the contributions on this topic are highly dependent on internal characteristics or physical properties of the damper; others demand too much computing time for real-time applications.

To cope with these drawbacks a novel method to model *ER* dampers is proposed. The method comprehends two sequential steps: a characterization procedure where the dynamical response of the damper is analyzed. Then a model customization procedure where a general model is particularized. The method needs experimental data of the *ER* damper under a specific *Design of Experiment* (*DoE*).

⋆ Authors thank *Autotronics* and *Development of Products for Emerging Markets* research chairs at *Tecnológico de Monterrey.*

This paper is organized as follows: In section 2 the experimental system and the *DoE* are shown. Section 3 describes the proposed characterization step. Section 4 presents the model customization step. Section 5 shows the identification step and in section 6 the validation method is defined. Section 7 presents the results and compares the performance of the customized model versus other reported model. Finally, section 8 concludes the paper highlighting the advantages of the proposed method.

2. EXPERIMENTAL SYSTEM

A commercial *ER* damper was used, it has a stroke of ± 150 mm and a continuous voltage input range from 0 to 5 kV. The force range is $[-2,500, 4,500]$ N. The *ER* damper is actuated by a *Fludicon*^{TM}*CarCon2*® module which is controlled by a *PWM* signal with frequency of 25 kHz and duty cycle range of $10\% - 80\%$.

The experimental setup consists of three modules: the acquisition module, which captures the displacement, velocity, damper force and *PWM* signals using a *NI*$^{\text{TM}}$*cDaq*; the actuation module which consists of a hydraulic piston that is actuated by a *MTS* 407 controller to command the displacement of the damper; and the control module that consists of a *NI*$^{\text{TM}}$*LabView*®control interface.

A series of displacement and actuation signal sequences, were used to capture the static and dynamic relations between velocity, displacement, and the damper force. These sequences ensure that the *ER* damper will be tested in relevant modes for realistic automotive applications. Table 1 shows the *DoE* for characterization and identification of the *ER* damper. Three replicas of each experiment were carried out.

The sequences used for the displacement of the piston were: *Road Profile* (*RP*), and *Decreasing-amplitude*

Table 1. Design of Experiments.

Exp.	Displacement			Actuation signal	Purpose
	Signal	Amp. [mm]	Freq. [Hz]		
E_1	*DSFS*	$\pm 1 - \pm 8$	[0.5-14.5]	*SC*	Charac.
E_2	*RP*	± 8	[0-3]	*PRBS*	Ident.
E_3	*RP*	$\pm 1 - \pm 8$	[0-3]	*ICPS*	Ident.
E_4	*DSFS*	$\pm 1 - \pm 8$	[0.5-14.5]	*ICPS*	Ident.
E_5	*DSFS*	$\pm 1 - \pm 8$	[0.5-14.5]	*PRBS*	Ident.

Stepped Frequency Sinusoidal signal (*DSFS*). The *RP* represents the motion in a vehicle suspension when the vehicle is driven through a specific surface. The *DSFS* signal is used to analyze the transient response of the *ER* damper and the hysteresis loops when changes in magnitude and frequency are present. The bandwidth of the *DSFS* includes the comfort and road holding specifications for automotive applications.

For the actuation signal (*PWM* duty cycle), were used: *Stepped inCrements* (*SC*) signal is used in the characterization of the *ER* damper to study the effect of the actuation signal. *Increased Clock Period Signal (ICPS)* and *Pseudo Random Binary Signal (PRBS)* sequences are used to analyze the damper transient response due to changes in the command signal.

3. CHARACTERIZATION

The *ER* damper force can be represented by two components: a passive component, which is present for all the damper input values, and a *SA* component which depends on the actuation input, (Dixon, 2007), as:

$$F_{SA}(V) = F_D(V) - F_P \tag{1}$$

where F_{SA} is the *SA* damper force, i.e. the force without the passive force F_P when a voltage V is applied. F_D is the measured damping force.

Based on experimental data the *Force-Velocity* (*FV*) and Force-Displacement (*FD*) diagrams are build. These experimental diagrams are analyzed to graphically identified some characteristics: hysteresis, static friction, viscous damping, stiffness and compressibility, Fig. 1(A,B). Afterwards, the *SA* diagrams are obtained using (1), the pre-yield and post-yield zones are identified, Fig. 1C. The *SA* phenomena includes: pre-yield and post-yield regions and hysteresis. At the yield point the damper fluid behavior changes from pseudo-plastic to quasi-solid, (Irgens, 2008). In the *FV* diagram the yield point is a cartesian point where the damping force becomes independent of the velocity. The yield point defines the zone where the *SA* damper operates: in pre-yield or in post-yield zone. Also, the average actuation signal that depends on the force gain (*FM*) is obtained.

3.1 Passive behavior.

Figure 2 shows significative effects that are present in the *ER* damper operating in passive mode. From the *FV* diagram, Fig. 2A, it can be seen that it is asymmetrical, the maximum force in extension is greater than the force generated in compression. The force has a component that depends on the velocity. The damper presents hysteresis in all its operational range, it is been more notorious at high

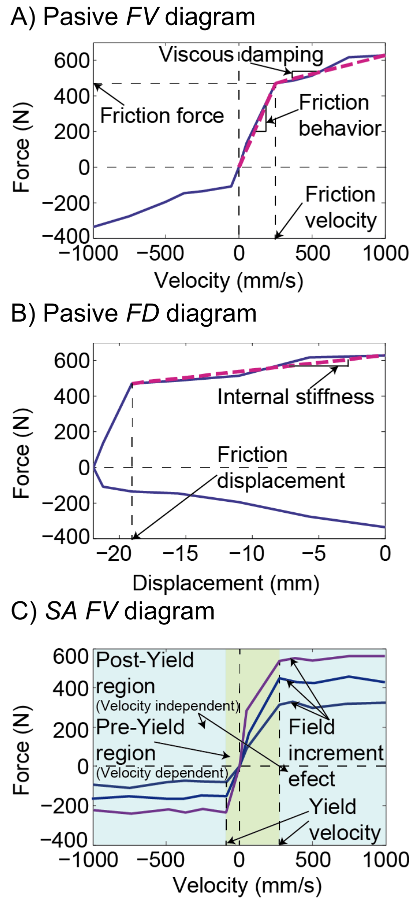

Fig. 1. Characteristic diagrams of a *SA* damper.

speeds in positive velocities, this suggests dependence on the frequency. At low speeds, high static friction (~ 700 N) is observed. This *ER* damper is subjected to a stick-slip phenomenon, specially in positive velocities; according to (Dixon, 2007) this phenomenon appears in the *ER* damper as a force overshot when the flow changes its direction. In the *FD* diagram, Fig. 2B, the stick-slip becomes more evident, as well as the effect of the frequency in the damper stiffness.

3.2 SA behavior

The behavior of the *SA* component of the force is shown in Fig. 3. The relation between the *SA* force and the *PWM* duty cycle becomes evident, Fig. 3A, this relationship is asymmetrical. In the post-yield region, Fig. 3B, the force is almost independent of the piston velocity, but in the pre-yield zone the force is highly influenced by the velocity. At low speed the hysteresis loop in *SA* force is not significant; but, as the velocity and the *PWM* duty cycle rises, the hysteresis is affected. The *Force-Manpulation* (*FM*) diagram shows that the average force gain for this particular *ER* damper has a linear pattern.

4. MODEL CUSTOMIZATION

After the characterization step, the model structure must be customized. Equations (2), (3) and (4) represent the general *SA* model, which includes almost all the observed phenomena in *SA* dampers.

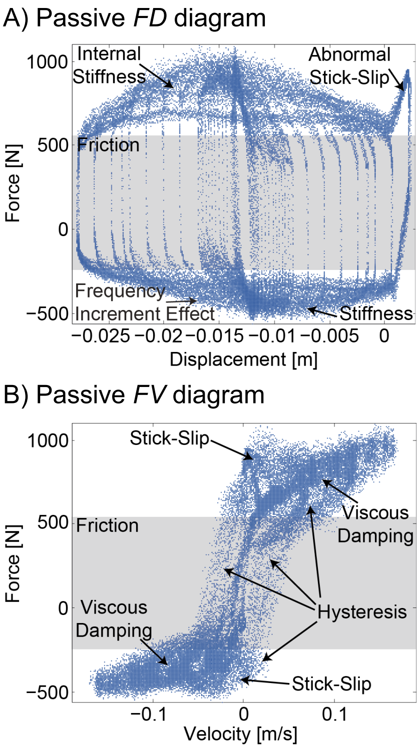

Fig. 2. Characteristic diagrams in passive behavior.

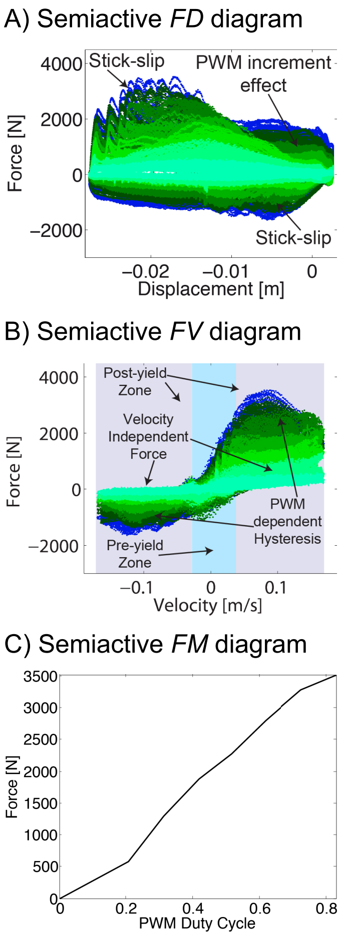

Fig. 3. Characteristic diagrams in semiactive behavior.

Table 2. Model terms used to represent *ER* damper characteristics.

Characteristic	Diagram in which is observed	Model term
Viscous damping.	Passive FV	$c_\mathrm{p}\dot{z}$
Stiffness.	Passive FD	$k_\mathrm{p}z$
Friction.	Passive FV	f_fr
Hysteresis loop.	Passive FV	$f_\mathrm{h,z}$
Frequency dependent hysteresis loop.	Passive FV	$f_{\mathrm{h},\dot{z}}$, m_D
Pre-yield zone.	SA FV	$f_{\mathrm{pre-y},\dot{z}}\mathrm{V}$
Gain in force due to manipulation.	SA FV	c_SA

$$F_\mathrm{D}(V) = F_\mathrm{P} + F_\mathrm{SA}(V) \tag{2}$$

where:

$$F_\mathrm{P} = f_0 + c_\mathrm{p}\dot{z} + k_\mathrm{p}z + m_\mathrm{D}\ddot{z} + f_\mathrm{fr} + f_\mathrm{h,z} + f_{\mathrm{h},\ddot{z}} \tag{3}$$

$$F_\mathrm{SA}(V) = V c_\mathrm{SA}\left[f_{\mathrm{pre-y},\dot{z},\mathrm{V}} + f_\mathrm{pre-y,z}\right] \tag{4}$$

with:

$$f_\mathrm{fr} = f_\mathrm{f}\left(\frac{v_\mathrm{f}\dot{z} + x_\mathrm{f}z}{1 + |v_\mathrm{f}\dot{z} + x_\mathrm{f}z|}\right) \tag{5a}$$

$$f_\mathrm{h,z} = f_\mathrm{h,z}\left(\frac{v_\mathrm{h,z}\dot{z} + x_\mathrm{h,z}sign(z)}{1 + |v_\mathrm{h,z}\dot{z} + x_\mathrm{h,z}sign(z)|}\right) \tag{5b}$$

$$f_{\mathrm{h},\ddot{z}} = f_{\mathrm{h},\ddot{z}}\left(\frac{v_{\mathrm{h},\ddot{z}}\dot{z} + x_{\mathrm{h},\ddot{z}}sign(\ddot{z})}{1 + |v_{\mathrm{h},\ddot{z}}\dot{z} + x_{\mathrm{h},\ddot{z}}sign(\ddot{z})|}\right) \tag{5c}$$

$$f_{\mathrm{pre-y},\dot{z},\mathrm{V}} = \left(\frac{v_{\mathrm{pre-y},\dot{z},\mathrm{I}}\dot{z} * V}{1 + |v_{\mathrm{pre-y},\dot{z},\mathrm{I}}\dot{z} * V|}\right) \tag{5d}$$

$$f_\mathrm{pre-y,z} = \left(\frac{x_\mathrm{pre-y,z}z}{1 + |x_\mathrm{pre-y,z}z|}\right) \tag{5e}$$

Equation (3) describes the passive force (F_P) The component f_0 is an initial compensation force generated by the accumulator; c_p is the viscous damping coefficient which describes the linear viscous damping of the Newtonian fluids; k_p is the stiffness coefficient which is the characteristic of linear elastomers; m_D is the virtual damper mass; f_fr is the damping force due to friction and $f_\mathrm{h,z}$,$f_{\mathrm{h},\dot{z}}$ model the hysteresis, (Guo et al., 2006; Cesmeci and Engin, 2006, 2010). Equation (4) represents the SA force $F_{SA}(V)$, where V is the manipulation applied to the damper, c_SA is the force gain due to manipulation and $f_\mathrm{pre-y,z}$, $f_{\mathrm{pre-y},\dot{z},\mathrm{I}}$ describe the behavior of the damper in the pre-yield zone. Because the SA damper has an asymmetric behavior the model needs different coefficients for positive and negative velocities. The general model is customized by including only the terms that mimics the observed characteristics during the previous step using the guidelines in Table 2.

The customized model ends:

$$F_\mathrm{D}(V) = F_\mathrm{P} + F_\mathrm{SA}(V) \tag{6a}$$

$$F_P = f_0 + c_p\dot{z} + k_p z + m_D\ddot{z} + f_{fr} \tag{6b}$$

$$F_{SA} = V c_{SA}\left[f_{pre-y,\dot{z},V} + f_{pre-y,z}\right] \tag{6c}$$

5. IDENTIFICATION

The parameters of model (6a, 6b, 6c) were fitted using a nonlinear *Least Squared Estimation* (*nLSE*) method based on the *Trust Region Reflective* algorithm. Three replicas of each experiment were used to evaluate the performance of the customized model. Fig. 4 shows the *FV*, *FD*, *FE* and *FT* diagrams obtained from E_2.

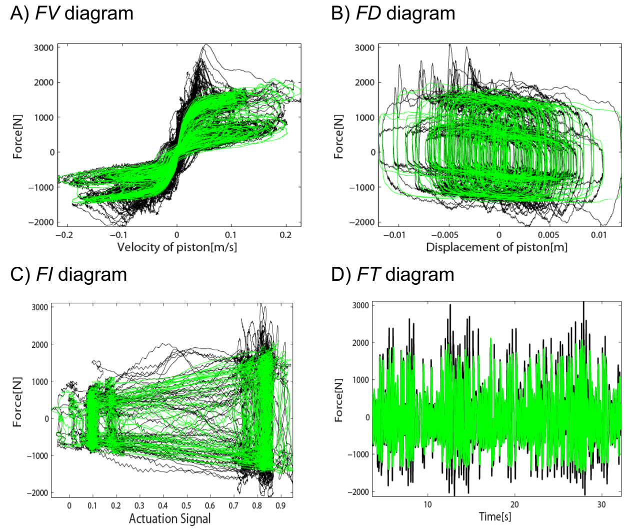

Fig. 4. Comparison of estimated (green) and real (black) data (E_2).

Qualitatively the customized model describes the nonlinear behavior of the *ER* damper. However, this model was unable describe the stick-slip phenomenon, thus it does not emulate the observed force peak around $0.04\,m/s$, Fig. 4A.

For quantitatively validation, the *Error to Signal Ratio ESR* was chosen as performance index. The *ESR* represents the ratio of variances of the estimation error and the experimental damper force, Savaresi et al. (2005):

$$ESR = \frac{\sum_{i=1}^{N}(F_{Di} - \hat{F}_{Di})^2}{\sum_{i=1}^{N}(F_{Di} - \frac{\sum_{j=1}^{N} F_{Dj}}{N})^2} \tag{7}$$

where N is the number of samples, F_{Di} is the real force and $\hat{F}_{Di}$ is the estimated force in the i-th sample. The value of the *ESR* is in the range of $[0, 1]$, where a value of 0 indicates that the model estimates exactly the damper force, whereas a value of 1 indicates that the model only predicts the mean value of the damper force. The performance indexes for all the experiments with the customized and full models are shown in Table 3. It can be observed that the values of the *ESR* are consistent.

Table 3. *ESR* index detail for all 3 replicas of the full and customized models

Exp.	**Replica 1**	**Replica 2**	**Replica 3**
	Customized Model		
E_2	0.0741	0.0749	0.0716
E_3	0.0620	0.0627	0.0654
E_4	0.1284	0.1337	0.1315
E_5	0.1558	0.1494	0.1416
	Full Model		
E_2	0.0730	0.0739	0.0719
E_3	0.0674	0.0661	0.0681
E_4	0.1258	0.1353	0.1330
E_5	0.0797	0.0762	0.0744

6. MODEL VALIDATION

The first step of the validation process is to prove that the terms discarded have little influence in the modeling performance, this is done by comparing the performance indexes obtained with the full model versus the customized model, Table 3 (first column).

have a grater *ESR* index than E_3 and E_4, respectively

Experiments with *ICPS* manipulation signal (E_3 and E_4) have smaller changes in the actuation signal, which has less effect in the variability of the force; in comparison than the ones with the *PRBS* manipulation signal (E_2 and E_5), which have grater *ESR* index caused by abrupt changes on the manipulation signal. This variability increments the effects of some phenomena like the stick-slip and hysteresis. Since in the model customization step those terms were excluded, the model is less effective to capture those hysteretic behaviors. This justify why in the experiment E_5 the *ESR* is almost double compared with the full model.

The second validation is related to the extrapolation. Table 4 compares results of the models obtained for one experiment versus the other experiments. Each vertical line describes which experiment was used to identification while the horizontal lines shows the experiment used for validation. In the diagonal it can be found the results of the identification step (first column of Table 3).

Table 4. Performance indices for different datasets using the customized *ER* model

Experiment validation	Force Variance $\sigma^2 \times 10^5$	Experiment Identification E_2	E_3	E_4	E_5
E_2	8.39	0.0741	0.0811	0.1988	0.1065
E_3	6.50	0.0676	0.0620	0.1762	0.1154
E_4	5.79	0.3041	0.0614	0.1258	0.1664
E_5	6.13	0.2546	0.3032	0.1727	0.1558
	Average	0.1751	0.1269	0.1684	0.1360

It was observed that the customized model can be extrapolated to other signals. The best average performance was obtained by the experiment E_5. This is because the *DSFS* signal captures better the dynamical behavior of the damper in its whole range of operation while the *RP* signal only explores a limited zone. The *ICPS* covers the whole force range of the shock absorber while the *PRBS* only captures the limits of the force range.

The customized model was also validated with a qualitative technique using 2D-density plots. The 2D-density plots use blue color to indicate a lower number of occurrences (data samples), whereas red indicates a higher number. The *FD*, *FV* and *FM* 2D-density plots obtained with the customized model are compared with the experimental ones, Fig. 5. Plots must have same shape a density distribution.

The zones with higher density of occurrences should be at low velocities of the *FV* diagram for the *RP* displacement signals. In the case of the *FD* diagrams these zones should be in the small displacement range, on the other hand this experiment has a *PRBS* actuation signal sequence; therefore, the higher density zones must be in the ends of the control signal (0.1 and 0.8). The *FV* diagram of the estimated data is similar the one obtained with experimental data, Fig. 5A,C. The shape and distribution of the real and estimated *FD* and *FM* diagrams are also similar; but because the stick-slip phenomenon is not considered

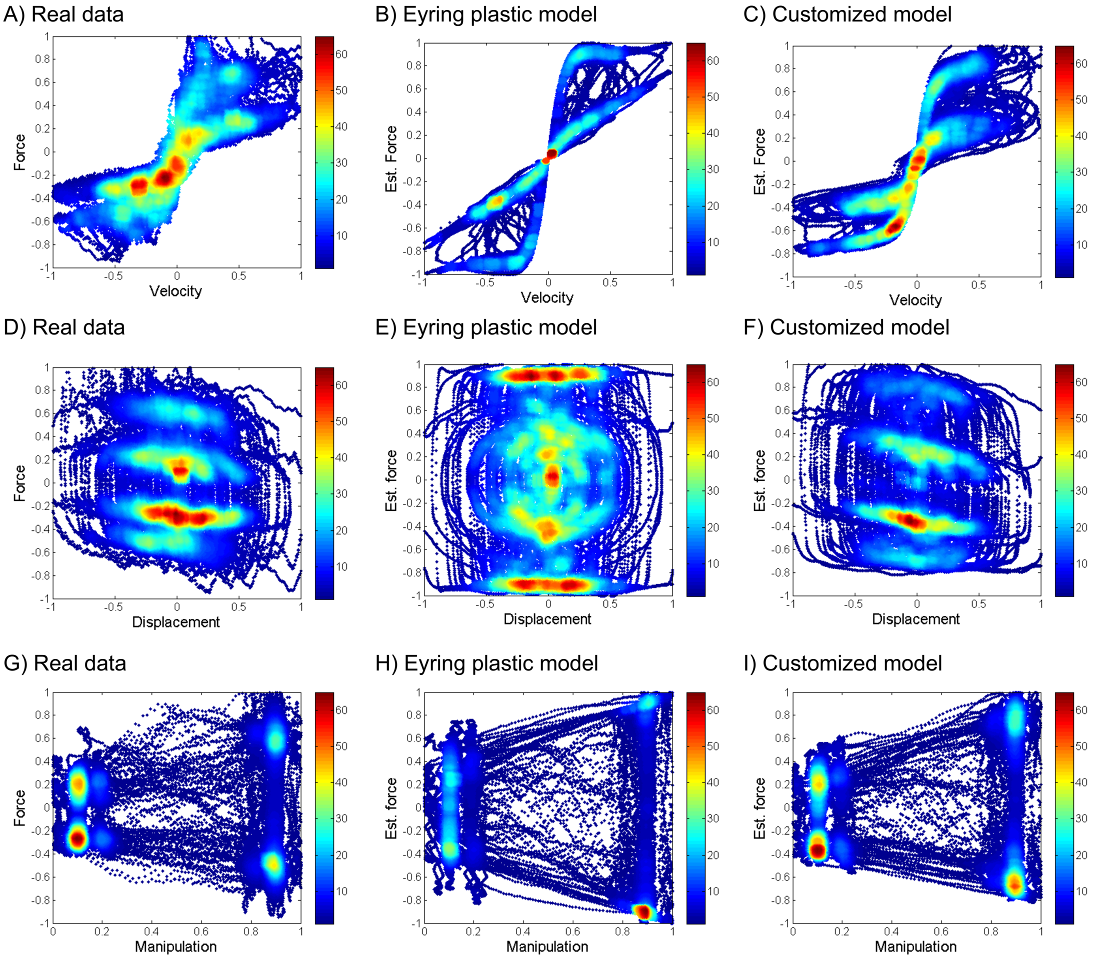

Fig. 5. 2D-density plots obtained with real data and estimated data with different *ER* damper models (E_2).

by the model, the estimated force does not present the peak around 0.04 m/s observed in experimental data.

7. RESULTS

In order to analyze the effectiveness of the customized model, a comparative analysis with the *Eyring*-plastic model, Bitman et al. (2005), is carried out. In this model, the force is considered as a non-linear function of the velocity:

$$F_{\mathrm{D}} = F_{\alpha}[arcsinh(\lambda_1 \dot{z} - \lambda_2 z)](1 + \beta_1 e^{-\beta_2|\dot{z}|}) + c_1\dot{z} + c_3\dot{z}^3 \quad (8)$$

where λ_1 is the slope of the response in the pre-yield region, λ_2 is the pre-yield hysteresis loop, F_α is related with the yield force amplitude, β_1, β_2 are yield force correction factors, and c_1 and c_3 model the damping in the post-yield region. Those parameters are functions of the excitation frequency and electric field. Table 5 compares the features of these models.

Both of the analyzed *ER* models are nonlinear and depend on the damper displacement z and velocity $\dot{z}$. Only the customized model includes the acceleration $\ddot{z}$ as input. In the *Eyrig*-plastic model the parameters are undefined functions of the actuation signal, and they were identified using the same nonlinear *LSE* method. Since these models were tested under same experimental conditions, it is possible to compare the models and determine the best model structure. The resulting performance indices are shown in Table 6. Analyzing the *ESR* index, the customized model had the best modeling performance for all experiments.

Table 5. Comparison of models

Model	Eyrig-plastic model	Customized model
Parameters	7	20
Inputs	z, $\dot{z}$	z, $\dot{z}$, $\ddot{z}$
Actuation signal as input	No	Yes
Hysteresis	Yes	Yes

Table 6. *ESR* indices of the *ER* damper models.

Model	Experiment		
	E_2	E_3	E_4
Eyring-plastic model	0.0996	0.0816	0.1996
Customized model	**0.0714**	**0.0642**	**0.1284**

Figure 6 compares the *FV* diagram obtained for each model in experiments E_3. The *Eyring*-plastic model has acceptable results at high velocities, but at low velocities ($\pm$0.02 m/s) it does not capture the hysteresis effect correctly. On the other hand, the customized model shows the best modeling performance since the nonlinearities added by the manipulation signal are described and the low and high damping forces are correctly identified. None of the analyzed models consider the stick-slip effect so the peak in the experimental force around 0.04 m/s is not emulated by any of them.

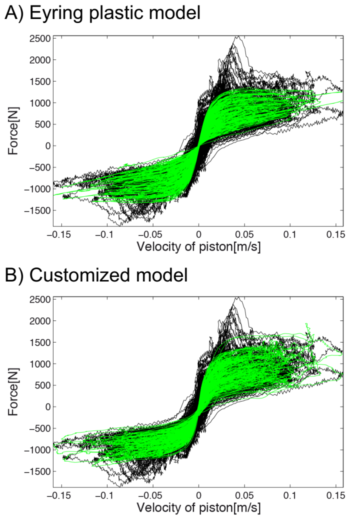

Fig. 6. Comparison of models based on FV diagrams. Real (black) versus estimated (green) data.

These models are also qualitatively compared using 2D-density plots in order to identify if these models predict correctly the distribution of the experimental data. Fig. 5 presents a comparison of the 2D-density plots of the experiment E_2. In the experimental FV diagram, Fig. 5A, the higher density of data appears with small compression forces while in the *Eyring*-plastic model FV diagram, Fig. 5B, the higher density appears with zero force, therefore the model generates smaller forces than the real damper with low velocities. Meanwhile, the customized model, Fig. 5C, generates a similar density of experimental data for extension forces and slightly larger compression forces.

In the FD diagram the experimental data presents higher density with small forces, especially in compression, Fig. 5D. In the *Eyring*-plastic model the higher density appears with large forces and exhibits a saturation, Fig. 5E, hence this model produces smaller forces with large displacements than the real damper. Finally, the customized model, Fig. 5F, produces slightly higher forces at low frequencies and a density distribution similar to the real data.

The FM diagram is important for control systems purposes. A model with the same shape and density distribution to the experimental data is required in order to compute a right manipulation to achieve a desired force. Since in experiment E_2 a $PRBS$ actuation signal was used, the FM diagram mostly exhibits two manipulation values, Fig. 5G. All the models generate smaller forces with a manipulation of 90% where the stick-slip effect is more evident. Nonetheless, the FM diagram obtained with the customized model resembles the real data. The *Eyring*-plastic model presents smaller forces than the customized model.

8. CONCLUSIONS

A new method for modeling ER dampers was proposed. This method does not need any priory knowledge of the damper to be modeled, just experimental data. The main contribution of this method is by just analyzing plots based on real data, the ER damper can be characterized and customized to get an efficient model that captures the real behavior of a damper.

An experimental setup was mounted with a commercial damper to obtain characteristic real diagrams.

The resultant model proves its accuracy by reproducing the nonlinear behavior of the damper with an ESR of 15.5% in the worst case and an average of 12.7% when is used to extrapolate the force of other experiments. Also, compared with other models the customized model has better performance, i.e. it has on average 28.4% less ESR than the *Eyring*-plastic model. Finally the 2D-density plots show that the model captures the characteristic behavior of a real shock absorber under normal operating conditions.

REFERENCES

Bitman, L., Choi, Y.T., Choi, S.B., and Wereley, N.M. (2005). Electrorheological Damper Analysis Using an Eyring-Plastic Model. *Smart Mater Struct*, 14(1), 237–246.

Cesmeci, S. and Engin, T. (2006). A Novel Hysteretic Model for Magnetorheological Fluid Dampers and Parameter Identification Using Particle Swarm Optimization. *Sensors and Actuators A: Physical*, 132(2), 441 – 451.

Cesmeci, S. and Engin, T. (2010). Modeling and Testing of a Field-Controllable Magnetorheological Fluid Damper. *Int J Mech Sci*, 52(8), 1036 – 1046.

Chen, S.M. and Wei, C.G. (2006). Experimental Study of the Rheological Behavior of Electrorheological Fluids. *Smart Mater Struct*, 15(2), 371–377.

Choi, S.B., Han, Y.M., and Sung, K.G. (2008). Vibration Control of Vehicle Suspension System Featuring ER Shock Absorber. *Int J Appl Electrom*, 27(3), 189–204.

Dixon, J. (2007). *The Shock Absorber Handbook*. Wiley-PEPublishing Series. John Wiley & Sons.

Guo, S., Yang, S., and Pan, C. (2006). Dynamic Modeling of Magnetorheological Damper Behaviors. *J Intel Mat Syst Str*, 17(1), 3–14.

Hong, S.R., Choi, S.B., Choi, Y.T., and Wereley, N.M. (2005). A Hydro-Mechanical Model for Hysteretic Damping Force Prediction of ER Damper: Experimental Verification. *J Sound Vib*, 285(4-5), 1180–1188.

Irgens, F. (2008). *Continuum Mechanics*. Springer-Verlag Berlin Heidelberg.

Nguyen, Q. and Choi, S. (2009). A New Approach for Dynamic Modeling of an Electrorheological Damper using a Lumped Parameter Method. *Smart Mater Struct*, 18(11), 1–11.

Nguyen, S. and Choi, S. (2012). A New Neuro-Fuzzy Training Algorithm for Identifying Dynamic Characteristics of Smart Dampers. *Smart Mater Struct*, 21(8), 1–14.

Savaresi, S.M., Bittanti, S., and Montiglio, M. (2005). Identification of Semi-Physical and Black-Box Non-Linear Models: the Case of MR-Dampers for Vehicles Control. *Automatica*, 41(1), 113 – 127.

Stanway, R., Sproston, J.L., and El-Wahed, A.K. (1996). Applications of Electro-Rheological Fluids in Vibration Control: a Survey. *Smart Mater Struct*, 5(4), 464–482.